


Model-Based Control for Soft Robots With System Uncertainties and Input Saturation

Xiangyu Shao , Pietro Pustina , *Graduate Student Member, IEEE*, Maximilian Stölzle , Guanghui Sun , *Senior Member, IEEE*, Alessandro De Luca , Ligang Wu , *Fellow, IEEE*, and Cosimo Della Santina , *Senior Member, IEEE*

Abstract—Model-based strategies are a promising solution to the grand challenge of equipping continuum soft robots with motor intelligence. However, finite-dimensional models of these systems are inherently inaccurate, thus posing pressing robustness concerns. Moreover, the actuation space of soft robots is usually limited. This article aims at solving both these challenges by proposing a robust model-based strategy for the shape control of soft robots with system uncertainty and input saturation. The proposed architecture is composed of two key components. First, we propose an observer that estimates deviations between the theoretical model and the soft robot, ensuring that the estimation error converges to zero within finite time. Second, we introduce a sliding mode controller to regulate the

soft robot shape while fulfilling saturation constraints. This controller uses the observer's output to compensate for the deviations between the real system and the established model. We prove the convergence of the closed-loop with theoretical analysis and the method's effectiveness with simulations and experiments.

Index Terms—Disturbance observer, input saturation, model-based control, sliding mode control, soft robots.

I. INTRODUCTION

CONTINUUM soft robots are made of continuously deformable elements and are inspired by invertebrate animals [1]. With their peculiar characteristics, they are expected to execute tasks that are currently not achievable for standard rigid robots—for example, interacting with uncertain environments, possibly involving humans. Nevertheless, the soft robot's highly deformable nature that makes these tasks possible also makes their control challenging. As a result, soft robot motor intelligence is still minimal today.

In recent years, a rising interest has been building around model-based strategies as a possible solution to the soft robot control challenge [2], with encouraging accomplishments [3], [4], [5], [6], [7]. However, many unsolved issues still hinder the practical application of model-based methods. This article focuses on two relevant and often overlooked blocking issues: model uncertainty and control saturation. First, models for soft robots are inherently inaccurate. Indeed, although control-oriented dynamic models are getting more advanced [8], [9], they can never match the infinite-dimensional nature of their exact formulation [10]. Moreover, limitations in fabrication strategies introduce variability of behaviors. Second, commonly used actuation strategies in soft robotics (e.g., pressure, vacuum, electroactive polymers) are limited in the range [11], and the controller quickly incurs input saturation. When saturation occurs, the control performances usually deteriorate, sometimes even resulting in instabilities.

Sliding mode controllers (SMCs) have proven to be robust to uncertainties and able to achieve high accuracy and fast response times [12], [13]. Within the SMC field, observer-based methods have been widely investigated [14], [15]. Concerning robotics applications, [16] proposed a combination of a sliding perturbation observer and an SMC for a rigid manipulator, and

Manuscript received 4 February 2023; revised 9 June 2023; accepted 26 July 2023. This work was supported in part by the National Key R&D Program of China under Grant 2019YFB1312001, in part by the National Natural Science Foundation of China under Grant 62033005, Grant 62022030, and Grant 62003114, and in part by the Natural Science Foundation of Heilongjiang Province under Grant ZD2021F001. The work by Pietro Pustina and Alessandro De Luca was financially supported by the PNRR MUR project under Grant PE0000013-FAIR. The work by Maximilian Stölzle was supported by the European Union's Horizon Europe Program from Project EMERGE under Grant 101070918. (Pietro Pustina and Maximilian Stölzle contributed equally to this work.) (Corresponding author: Ligang Wu.)

Xiangyu Shao is with the School of Astronautics, Harbin Institute of Technology, Harbin 150001, China, and also with the Department of Cognitive Robotics, Delft University of Technology, 2628 CD Delft, The Netherlands (e-mail: xiangyushao@hit.edu.cn).

Pietro Pustina is with the Department of Cognitive Robotics, Delft University of Technology, 2628 CD Delft, The Netherlands, and also with the Department of Computer, Control and Management Engineering, University of Rome La Sapienza, 00185 Rome, Italy (e-mail: pietro.pustina@uniroma1.it).

Maximilian Stölzle is with the Department of Cognitive Robotics, Delft University of Technology, 2628 CD Delft, The Netherlands (e-mail: m.w.stolzle@tudelft.nl).

Guanghui Sun and Ligang Wu are with the School of Astronautics, Harbin Institute of Technology, Harbin 150001, China (e-mail: guanghuisun@hit.edu.cn; ligangwu@hit.edu.cn).

Alessandro De Luca is with the Department of Computer, Control and Management Engineering, University of Rome La Sapienza, 00185 Rome, Italy (e-mail: deluca@diag.uniroma1.it).

Cosimo Della Santina is with the Department of Cognitive Robotics, Delft University of Technology, 2628 CD Delft, The Netherlands, also with the Institute of Robotics and Mechatronics, German Aerospace Center (DLR), 82234 Oberpfaffenhofen, Germany, and also with the Department of Informatics, Technical University of Munich, 80333 Munich, Germany (e-mail: c.dellasantina@tudelft.nl).

Color versions of one or more figures in this article are available at <https://doi.org/10.1109/TIE.2023.3303636>.

Digital Object Identifier 10.1109/TIE.2023.3303636

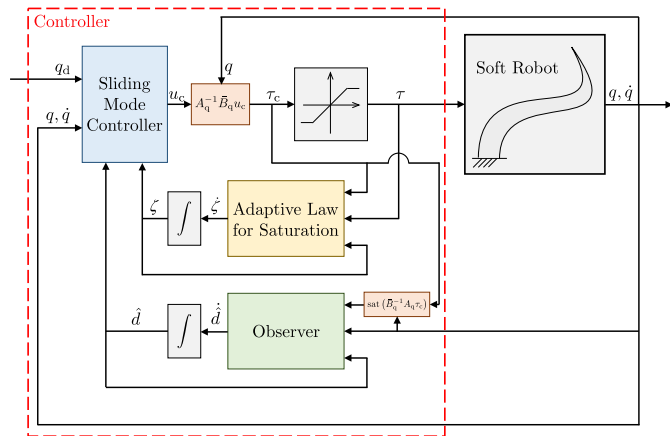


Fig. 1. Block scheme representation of the proposed control architecture. An SMC is fed with the output of an observer that estimates the deviation between the theoretical model and the real system, and with the output of an adaptive law that guarantees closed-loop stability despite input saturation. The output of the controller is then transformed into a set of generalized forces by suitable transformations.

Hamza et al. [17] used a similar strategy to achieve position control of an assistive robot. Regarding the application of SMC in soft robotics, [18], [19], [20] present encouraging results. However, most of them still use the traditional SMC framework, which relies on the upper bound knowledge of the system uncertainty to assure stability [21]. Moreover, none of them take input saturation into account.

In this article, we propose a control architecture (see Fig. 1) that simultaneously solves both challenges, with the goal of achieving reliable closed-loop behavior. The core of the method is a robust SMC, which in turn relies on two components that take care of uncertainty and input saturation. The first is a disturbance observer, whose output is used by the SMC as compensation. The second is an adaptive law to guarantee the system's stability with respect to input saturation. Considering the importance of disturbance observers for real-time compensation of system uncertainty [16], we leverage the observer-based SMC framework to achieve reliable model-based control of saturated soft robots. We exploit the finite-time stability of high-order sliding mode observers and continuous terminal SMC to improve closed-loop performance. More precisely, this article contributes to the state-of-the-art in model-based control of soft robots with:

- 1) an observer for uncertainty estimation of soft robots with finite-time stability properties;
- 2) a finite-time and nonsingular SMC for shape regulation of soft robots with saturation and uncertainty compensation;
- 3) simulations and experiments showcasing the superior performance of the method compared to SoA benchmarks;
- 4) the first experimental verification of closed-loop control based on the Δ -parameterization [22] of the PCC dynamics [23].

II. MATHEMATICAL FORMULATION

A generic soft robot modeled by means of some discretization technique can be described [2] by ordinary differential equations

of the following form:

$$B_q \ddot{q} + C_{q,\dot{q}} \dot{q} + G_q + K_q q + D_q \dot{q} = A_q \tau \quad (1)$$

where $q, \dot{q}, \ddot{q} \in \mathbb{R}^n$ are the vector of configuration variables together with their first and second order time derivatives, $B_q \in \mathbb{R}^{n \times n}$ is the inertia matrix, $C_{q,\dot{q}}$ collects Coriolis and centrifugal terms, $G_q \in \mathbb{R}^n$ models gravitational effects, and $K_q \in \mathbb{R}^{n \times n}$ and $D_q \in \mathbb{R}^{n \times n}$ are the stiffness and damping matrices, respectively. $A_q \in \mathbb{R}^{n \times n}$ maps the input forces and torques $\tau \in \mathbb{R}^n$ to configuration space, causing the system to be fully actuated.

To account for the uncertainty that characterizes the model [2], we split the dynamic terms into known and unknown parts, i.e., $B_q = \bar{B}_q + \delta B_q$, $C_{q,\dot{q}} = \bar{C}_{q,\dot{q}} + \delta C_{q,\dot{q}}$, $G_q = \bar{G}_q + \delta G_q$, $K_q = \bar{K}_q + \delta K_q$, and $D_q = \bar{D}_q + \delta D_q$. Consequently, (1) can be rewritten as

$$\bar{B}_q \ddot{q} + \bar{C}_{q,\dot{q}} \dot{q} + \bar{G}_q + \bar{K}_q q + \bar{D}_q \dot{q} = A_q \tau + \delta \mathcal{F} \quad (2)$$

with $\delta \mathcal{F} = -\delta B_q \ddot{q} - \delta C_{q,\dot{q}} \dot{q} - \delta G_q - \delta K_q q - \delta D_q \dot{q}$. Model (2) verifies a set of well-known properties of classical rigid robots [22], [24], among these the following will be exploited in the remainder.

Property 1: The inertia matrix \bar{B}_q is symmetric and positive definite. Furthermore, there exist constants $b_1, b_2 > 0$ such that $b_1 \|q\|^2 \leq q^T \bar{B}_q q \leq b_2 \|q\|^2$ for all q .

Property 2: If the matrix $\bar{C}_{q,\dot{q}}$ is defined through Christoffel symbols, then $\dot{\bar{B}}_q = \bar{C}_{q,\dot{q}} + \bar{C}_{q,\dot{q}}^T$. In addition, there exist constants $c_1, c_2, c_3 > 0$ such that $\|\bar{C}_{q,\dot{q}}\| \leq (c_1 + c_2 \|q\| + c_3 \|\dot{q}\|^2) \|\dot{q}\|$ for all q and \dot{q} .

Assumption 1 [25]: The uncertainty $\delta \mathcal{F}$ is bounded and admits bounded first order time derivative $\delta \dot{\mathcal{F}}$, i.e., there exist constants $f_1, f_2 > 0$ such that $\|\delta \mathcal{F}\| \leq f_1$ and $\|\delta \dot{\mathcal{F}}\| \leq f_2$ for all q . Besides, we assume that the full-state feedback is available, i.e., the configuration q and its time derivative \dot{q} are fully observable.

III. CONTROL SCHEME

We present here our main contribution, the saturated disturbance observer-based sliding mode controller (DOSMC). As illustrated in Fig. 1, the scheme consists of an SMC, an observer to estimate the system uncertainty and disturbance, and an adaptive law to account for the input saturation and simultaneously guarantee closed-loop stability. Before diving into the details of the various elements of the scheme, we briefly list some lemmas that will be exploited in the stability analyses.

A. Preliminaries

Lemma 1 [26]: For the nonlinear system $\dot{x}(t) = f(x(t))$ with $f(0) = 0$ and $x(t) \in \mathbb{R}^n$, if one can find a Lyapunov function $V(x)$ satisfying $\dot{V}(x) \leq -\beta V^\gamma(x)$, $\beta > 0$, $0 < \gamma < 1$, then the system is finite-time stable with the settling time $T \leq \frac{1}{\beta(1-\gamma)} V^{1-\gamma}(x_0)$.

Lemma 2 [27]: For the system presented in Lemma 1, if the Lyapunov function $V(x)$ satisfying $\dot{V}(x) + \alpha V(x) + \beta V^\gamma(x) \leq 0$, $\alpha > 0$, $\beta > 0$, $0 < \gamma < 1$, then for any initial

state $V(x_0)$, the solution of the system converges within time $T = \frac{1}{\alpha(1-\gamma)} \ln \frac{\alpha V^{1-\gamma}(x_0) + \beta}{\beta}$.

Lemma 3 [28]: For the system presented in Lemma 1, if the Lyapunov function $V(x)$ satisfies $\dot{V}(x) \leq -\alpha V(x) - \beta V^\gamma(x) + \eta$, in which $\alpha, \beta > 0$, $0 < \gamma < 1$, $0 < \eta < \infty$, then the solution of $f(x)$ will converge to the set $\Pi \triangleq \{x \mid V(x) \leq \min\{\frac{\eta}{(1-\chi)\alpha}, (\frac{\eta}{(1-\chi)\beta})^{\frac{1}{\gamma}}\}\}$ within time $T \leq \max\{\frac{1}{\alpha\chi(1-\gamma)} \ln \frac{\alpha\chi V^{1-\gamma}(x_0) + \beta}{\alpha\chi V^{1-\gamma}(x_T) + \beta}, \frac{1}{\alpha(1-\gamma)} \ln \frac{\alpha V^{1-\gamma}(x_0) + \beta\chi}{\alpha V^{1-\gamma}(x_T) + \beta\chi}\}$, in which $0 < \chi < 1$, $V(x_T)$ is the value of $V(x)$ at $t = T$.

In the following, define $\text{sat}(x) = \max(x_{\min}, \min(x, x_{\max}))$ as the saturation function where x_{\max} and x_{\min} are the lower and upper bounds of x , and $\text{sgn}(x) = \{0 \text{ if } x = 0; |x|/x \text{ otherwise}\}$ the sign function. Furthermore, given two vectors $v = [v_1 \cdots v_n]^T$ and $\gamma = [\gamma_1 \cdots \gamma_n]^T$, the operator $\text{sig}(v)^\gamma$ is defined as $\text{sig}(v)^\gamma = [|v_1|^{\gamma_1} \text{sgn}(v_1), \cdots, |v_n|^{\gamma_n} \text{sgn}(v_n)]^T$.

B. Observer Design

Property 1 allows to write the system dynamics (2) in its state space form

$$\dot{x}_1 = x_2, \quad \dot{x}_2 = F(x_1, x_2, t) + u + d \quad (3)$$

where $x_1 = q$, $x_2 = \dot{q}$, $F(x_1, x_2, t) = -\bar{B}_q^{-1}(\bar{C}_q \dot{q} + \bar{G}_q + \bar{K}_q q + \bar{D}_q \dot{q})$, $u = \bar{B}_q^{-1} A_q \tau$ stands for the control input and $d = \bar{B}_q^{-1}(\delta\mathcal{F} + \tau_d)$ represents the lumped uncertainty. To estimate d , the following observer can be used:

$$\begin{aligned} \dot{\hat{x}}_2 &= k_1 \Phi_1(x_2, \hat{x}_2) + F(x_1, x_2, t) + u + \hat{d} \\ \dot{\hat{d}} &= k_2 \Phi_2(x_2, \hat{x}_2) \end{aligned} \quad (4)$$

where $k_1, k_2 > 0$ are diagonal matrices, \hat{x}_2 and \hat{d} are the estimates of x_2 and d , respectively. $\Phi_1(x_2, \hat{x}_2) = \text{sig}(x_2 - \hat{x}_2)^{\frac{1}{2}} + \mu \text{sig}(x_2 - \hat{x}_2)^{\frac{3}{2}}$, $\Phi_2(x_2, \hat{x}_2) = \frac{1}{2} \text{sgn}(x_2 - \hat{x}_2) + 2\mu(x_2 - \hat{x}_2) + \frac{3}{2}\mu^2 \text{sig}(x_2 - \hat{x}_2)^2$ with $\mu > 0$ a diagonal matrix. The following result shows that \hat{x}_2 and \hat{d} converge to x_2 and d in finite time.

Theorem 1: Considering system (2) and its state-space form (3), the proposed observer (4) ensures that the estimation error converges to zero in finite time.

Proof: Taking (4) into (3) yields the error dynamics of the observer

$$\dot{\tilde{x}}_2 = -k_1 \Phi_1(x_2, \hat{x}_2) + \tilde{d}, \quad \dot{\tilde{d}} = -k_2 \Phi_2(x_2, \hat{x}_2) + \dot{\tilde{d}} \quad (5)$$

where $\tilde{x}_2 = x_2 - \hat{x}_2$ and $\tilde{d} = d - \hat{d}$ are estimation errors of x_2 and d .

Recalling that $d = \bar{B}_q^{-1} \delta\mathcal{F}$, from Properties 1–2 and Assumption 1, it follows that there exists a constant $d_c > 0$ s.t. $\|\tilde{d}\| \leq d_c$. Now define $\xi = [\varphi_{1i}, \tilde{d}_i]^T$, with φ_{1i} and \tilde{d}_i being the i th element of Φ_1 and \tilde{d} , respectively. Whenever $\tilde{x}_{2i} \neq 0$, the time derivative of ξ can be computed as

$$\dot{\xi} = \begin{bmatrix} \dot{\varphi}_{1i} \\ \dot{\tilde{d}}_i \end{bmatrix} = \begin{bmatrix} \varphi'_{1i} (-k_{1i} \varphi_{1i} + \tilde{d}_i) \\ -k_{2i} \varphi'_{1i} \varphi_{1i} + \dot{\tilde{d}}_i \end{bmatrix} \quad (6)$$

with $\varphi'_{1i} = \frac{1}{2} |\tilde{x}_{2i}|^{-\frac{1}{2}} + \frac{3}{2} \mu_i |\tilde{x}_{2i}|^{\frac{1}{2}}$ the partial derivation of φ_{1i} with respect to \tilde{x}_{2i} . Writing (6) in the matrix form yields

$$\dot{\xi} = \varphi'_{1i} (A\xi + B\varrho_i(\xi, t)) \quad (7)$$

where $A = [-k_{1i} \ 1; -k_{2i} \ 0]$, $B = [0 \ 1]^T$, and $\varrho_i(\xi, t) = \frac{\dot{\tilde{d}}_i}{\varphi'_{1i}} = \frac{2\tilde{d}_i \text{sgn}(\tilde{x}_{2i})}{(1+3\mu_i |\tilde{x}_{2i}|)(1+\mu_i |\tilde{x}_{2i}|)} \varphi_{1i}$. Being $\dot{\tilde{d}}$ bounded, there exists a constant $\delta_i > 0$ such that $\delta_i^2 \varphi_{1i}^2 - \varrho_i^2(\xi, t) \geq 0$. We claim that both φ_{1i} and \tilde{d}_i converge to zero in finite time. To show this, consider the Lyapunov candidate $V_1(\tilde{x}_{2i}, \tilde{d}_i) = \xi^T \Lambda \xi$, where $\Lambda = \Lambda^T$ is a positive definite matrix. Exploiting (7), $\dot{V}_1 = \dot{\xi}^T \Lambda \xi + \xi^T \Lambda \dot{\xi}$ can be bounded by

$$\dot{V}_1 \leq \varphi'_{1i} \begin{bmatrix} \xi \\ \varrho_i \end{bmatrix} \begin{bmatrix} A^T \Lambda + \Lambda A + L & \Lambda B \\ B^T \Lambda & -1 \end{bmatrix} \begin{bmatrix} \xi \\ \varrho_i \end{bmatrix} \quad (8)$$

with $L = \delta_i^2 C^T C$ and $C = [1 \ 0]$. Consider now the following linear matrix inequality:

$$\begin{bmatrix} A^T \Lambda + \Lambda A + L + \epsilon I & \Lambda B \\ B^T \Lambda & -1 \end{bmatrix} \leq 0 \quad (9)$$

where $\epsilon > 0$. According to [29], (9) is feasible i.f.f. the control gains $(k_{1i}, k_{2i}) \in K^+ = \{(k_{1i}, k_{2i}) \in \mathbb{R}^+ \mid k_{1i}^2 > 2k_{2i}, k_{2i} > \delta \vee k_{1i}^2 < 2k_{2i}, k_{1i}^2(4k_{2i} - k_{1i}^2) > (2\delta_i)^2\}$.

Exploiting the inequalities $V_1^{1/2}/\lambda_{\max}(\Lambda) \leq \|\xi\|_2 \leq V_1^{1/2}/\lambda_{\min}(\Lambda)$, $|\tilde{x}_{2i}|^{1/2} \leq \|\xi\|_2$, and the fact that (9) bounds from above the matrix appearing in the right-hand side of (8), \dot{V}_1 can be bounded by

$$\begin{aligned} \dot{V}_1 &\leq -\epsilon \varphi'_{1i} \|\xi\|_2^2 = -\frac{\epsilon \|\xi\|_2^2}{2|\tilde{x}_{2i}|^{\frac{1}{2}}} - \frac{3}{2} \epsilon \mu_i |\tilde{x}_{2i}|^{\frac{1}{2}} \|\xi\|_2^2 \\ &\leq -\frac{\epsilon}{2\lambda_{\max}(\Lambda)} V_1^{\frac{1}{2}} \end{aligned} \quad (10)$$

where $\lambda_{\min}(\Lambda)$ and $\lambda_{\max}(\Lambda)$ denote the smallest and largest eigenvalue of Λ , respectively. All the hypotheses of Lemma 1 are therefore verified, and both φ_{1i} and \tilde{d}_i converge to zero in finite time. Since the abovementioned reasoning holds for all i , Φ_1 and \tilde{d} converge to zero in finite time. The thesis follows noting that $\Phi_1 = 0$ implies $\tilde{x}_2 = 0$. ■

Remark 1: In the proof of Theorem 1, it is assumed $\tilde{x}_{2i} \neq 0$. To evaluate the stability of the error dynamics when $\tilde{x}_{2i} = 0$ but $\tilde{d}_i \neq 0$, we consider two different cases, i.e., $\tilde{x}_{2i} = 0$ in an entire time interval $[t_1, t_2]$ or at some instant of time $t_1 \geq 0$. If $\tilde{x}_{2i}(t) = 0$ for $t \in [t_1, t_2]$, then $\dot{\tilde{x}}_{2i}(t) = 0$ in the same time window. From (5) this implies that also $\dot{\tilde{d}}_i = 0$. On the other hand, if $\tilde{x}_{2i} = 0$ only at some instant of time t_1 , then necessarily $\dot{\tilde{x}}_{2i} \neq 0$ from which it follows that there exists $t_2 > t_1$ such that $\tilde{x}_{2i}(t_2) \neq 0$. Thus, we fall in the case $\tilde{x}_{2i} \neq 0$.

C. Controller Design for Saturated Soft Robots

Considering the input saturation in (3), one has

$$\dot{x}_1 = x_2, \quad \dot{x}_2 = F(x_1, x_2, t) + \text{sat}(u_c) + d \quad (11)$$

where $u = \text{sat}(u_c) \in [u_{\min}, u_{\max}]$ accounts for input saturation, with u_c being the virtual control inputs to be designed. Generally, the saturation exists in τ instead of u , i.e., $\tau \in [\tau_{\min}, \tau_{\max}]$. Whereas, given a set of system states, the saturation in τ and u can be easily mapped to each other with $u = \bar{B}_q^{-1} A_q \tau$. Note that both u_{\min} and u_{\max} are time-varying. However, as it will be shown next, this does not affect closed-loop stability.

To achieve configuration-space control, the following sliding surface is proposed:

$$s = \dot{e} + \alpha e + \beta s_\nu(e) \quad (12)$$

where $e = q - q_d$, q_d is a constant desired reference for q and $s_\nu(e)$ is defined as

$$s_\nu(e) = \begin{cases} \text{sig}(e)^\nu, & \bar{s} = 0 \cup \bar{s} \neq 0, |e| \geq \delta \\ \iota_1 e + \iota_2 e^2 \text{sgn}(e), & \bar{s} \neq 0, |e| < \delta \end{cases}$$

in which $\iota_1 = (2 - \nu)\delta^{\nu-1}$ and $\iota_2 = (\nu - 1)\delta^{\nu-2}$ ensure the continuity and derivability of s_ν [30], $\alpha > 0$, $\beta > 0$, $0.5 < \nu < 1$, $\delta > 0$, and $\bar{s} = \dot{e} + \alpha e + \beta \text{sig}(e)^\nu$ is the standard terminal sliding surface. The time derivative of s is given by

$$\dot{s} = \ddot{e} + \alpha \dot{e} + \beta \dot{s}_\nu. \quad (13)$$

Without input saturation, the controller to reach the sliding surface would have been defined as

$$u_1 = -F(x_1, x_2, t) + \ddot{q}_d - (\beta \dot{s}_\nu + \alpha \dot{e} + \kappa_1 s + \kappa_2 \text{sig}^\rho(s)) - \hat{d}. \quad (14)$$

However, we add an extra term to u_1 to compensate for the input saturation obtaining

$$u_c = -F(x_1, x_2, t) + \ddot{q}_d - \{\beta \dot{s}_\nu + \alpha \dot{e} + \kappa_1 s + \kappa_2 \text{sig}^\rho(s)\} - \hat{d} + k_\zeta \zeta \quad (15)$$

in which ζ evolves according to

$$\dot{\zeta} = \begin{cases} \Delta u - \bar{h}_1 \zeta - \bar{h}_2 \text{sig}^\rho(\zeta) - \frac{s^T \Delta u + \frac{\|\Delta u\|^2}{2}}{\|\zeta\|^2} \zeta, & \|\zeta\| > \sigma \\ 0, & \|\zeta\| \leq \sigma \end{cases} \quad (16)$$

where $\Delta u = \text{sat}(u_c) - u_c$, k_ζ is a positive definite matrix and $\sigma > 0$ is a user defined constant. We can now state the following result.

Theorem 2: Considering a saturated soft robot (11) with the designed observer (4) and the control law (15), the configuration space position will converge to a neighborhood of its equilibrium points in finite time.

Proof: Substituting (15) into (11), we have

$$\begin{aligned} \dot{x}_2 &= F(x_1, x_2, t) + u_c + \Delta u + d \\ &= -\{\beta \nu |e|^{\nu-1} \dot{e} + \kappa_1 s + \kappa_2 \text{sig}^\rho(s) + \alpha \dot{e}\} \\ &\quad + k_\zeta \zeta + d - \hat{d} + \Delta u. \end{aligned} \quad (17)$$

Then, (13) can be rewritten as

$$\dot{s} = -\{\kappa_1 s + \kappa_2 \text{sig}^\rho(s)\} + k_\zeta \zeta + (d - \hat{d}) + \Delta u. \quad (18)$$

For ease of reading, we divide the remaining part of the proof into three steps.

Step 1: The stability of the adaptive law (16) is easily proven with the Lyapunov candidate $V_2 = \frac{1}{2} \zeta^T \zeta$. In the case of $\|\zeta\| > \sigma$, its time derivative satisfies

$$\begin{aligned} \dot{V}_2 &\leq -\bar{h}_1 \|\zeta\|^2 - \bar{h}_2 \|\zeta\|^{\rho+1} + \|\zeta\| \|\Delta u\| + \|s\| \|\Delta u\| - \frac{1}{2} \|\Delta u\|^2 \\ &\leq -\left(\bar{h}_1 - \frac{1}{2}\right) \|\zeta\|^2 - \bar{h}_2 \|\zeta\|^{\rho+1} + \|s\| \|\Delta u\| \\ &\leq -\bar{h}_1 V_2 - \bar{h}_2 V_2^{\frac{1+\rho}{2}} + \Sigma \end{aligned} \quad (19)$$

where $\bar{h}_1 = 2h_1 - 1$, $\bar{h}_2 = 2^{\frac{\rho+1}{2}} h$, and $\Sigma = \|s\| \|\Delta u\|$. According to (12) and (15), s and Δu are bounded. Thus, from Lemma 3, ζ is finite-time stable if $\|\zeta\| > \sigma$, and its convergence region $\Psi \triangleq \{\zeta \mid \|\zeta\| \leq \max\{(\frac{\Sigma}{(1-\chi_1)\bar{h}_1})^{\frac{1}{2}}, \sigma\}\}$ decreases with the convergence of s and Δu . If $\|\zeta\| \leq \sigma$ then $\dot{\zeta} = 0$ and $\zeta \in \Psi$.

Step 2: To prove the stability of the sliding mode surface, consider the following Lyapunov function:

$$V_3 = \frac{1}{2} s^T s + \frac{1}{2} \zeta^T \zeta. \quad (20)$$

Its time derivative is

$$\begin{aligned} \dot{V}_3 &= s^T \dot{s} + \zeta^T \dot{\zeta} \\ &= -\{\kappa_1 \|s\|^2 + \kappa_2 \|s\|^{\rho+1}\} + s^T \varepsilon + s^T k_\zeta \zeta + s^T \Delta u + \zeta^T \dot{\zeta} \\ &\leq -\{\kappa_1 \|s\|^2 + \kappa_2 \|s\|^{\rho+1}\} + \|s\| \|\varepsilon\| + \|s\| \|k_\zeta \zeta\| \\ &\quad + s^T \Delta u + \zeta^T \dot{\zeta} \end{aligned} \quad (21)$$

where $\varepsilon = \sup\{d - \hat{d}\}$ is the maximum estimation error of the observer. Once again we analyze separately the case when $\|\zeta\| > \sigma$ and $\|\zeta\| \leq \sigma$.

Case 1: $\|\zeta\| > \sigma$

Considering (16) and the inequality $2\|x\|\|y\| \leq \|x\|^2 + \|y\|^2$, \dot{V}_3 can be upper bounded by

$$\begin{aligned} \dot{V}_3 &\leq -\{\kappa_1 \|s\|^2 + \kappa_2 \|s\|^{\rho+1}\} + \|s\|^2 + \frac{1}{2} \|\varepsilon\|^2 + \frac{1}{2} \|k_\zeta \zeta\|^2 \\ &\quad + \{-\bar{h}_1 \|\zeta\|^2 - \bar{h}_2 \|\zeta\|^{\rho+1} - s^T \Delta u - \frac{1}{2} \Delta u^T \Delta u \\ &\quad + \zeta^T \Delta u\} + s^T \Delta u \\ &\leq -\{(\kappa_1 + 1) \|s\|^2 + \kappa_2 \|s\|^{\rho+1}\} + \frac{1}{2} \|\varepsilon\|^2 + \frac{1}{2} \|k_\zeta \zeta\|^2 \\ &\quad + \{-\bar{h}_1 \|\zeta\|^2 - \bar{h}_2 \|\zeta\|^{\rho+1} + \frac{1}{2} \|\zeta\|^2\} \\ &\leq -\bar{\kappa}_1 (\|s\|^2 + \|\zeta\|^2) - \bar{\kappa}_2 (\|s\|^{\rho+1} + \|\zeta\|^{\rho+1}) + \frac{1}{2} \|\varepsilon\|^2 \end{aligned} \quad (22)$$

with $\bar{\kappa}_1 = \min\{\kappa_1 + 1, \frac{1}{2} k_\zeta + \bar{h}_1\}$, $\bar{\kappa}_2 = \min\{\kappa_2, \bar{h}_2\}$. Exploiting the inequality $(|r_1| + |r_2| + \dots + |r_n|)^p \leq |r_1|^p + |r_2|^p + \dots + |r_n|^p$, $0 < p < 1$, one has

$$-(\|s\|^{\rho+1} + \|\zeta\|^{\rho+1}) \leq -(\|s\|^2 + \|\zeta\|^2)^{\frac{\rho+1}{2}}. \quad (23)$$

Therefore, (22) yields

$$\dot{V}_3 \leq -\hat{\kappa}_1 V_3 - \hat{\kappa}_2 V_3^{\frac{\rho+1}{2}} + \frac{1}{2} \|\varepsilon\|^2 \quad (24)$$

where $\hat{\kappa}_1 = 2\bar{\kappa}_1$, $\hat{\kappa}_2 = 2^{\frac{\rho+1}{2}}\bar{\kappa}_2$. By Theorem 1, ε approaches zero in finite time. Thus, from (24) in finite time we have $\dot{V}_3 \leq -\hat{\kappa}_1 V_3 - \hat{\kappa}_2 V_3^{\frac{\rho+1}{2}}$ which implies, according to Lemma 2, the finite-time stability of s . Assume now that $\varepsilon \neq 0$, which can happen before the observer is stable or if the observer has static errors. In this case (24) can be rewritten as

$$\dot{V}_3 \leq -\chi\hat{\kappa}_1 V_3 - (1-\chi)\hat{\kappa}_1 V_3 - \hat{\kappa}_2 V_3^{\frac{\rho+1}{2}} + \frac{1}{2} \|\varepsilon\|^2 \quad (25)$$

where $0 < \chi < 1$. If $V_3 > \frac{\|\varepsilon\|}{2(1-\chi)\hat{\kappa}_1}$, one has $\dot{V}_3 \leq -\chi\hat{\kappa}_1 V_3 - \hat{\kappa}_2 V_3^{\frac{\rho+1}{2}}$ which implies that s converges in finite time to the set $\Pi_1 \triangleq \{(s, \zeta) \mid V_3(s, \zeta) \leq \frac{\|\varepsilon\|}{2(1-\chi)\hat{\kappa}_1}\}$. Recalling that \hat{d} is always bounded, also ε will be bounded. However, ε will be much smaller than d after the observer is stabilized, which leads s to converge to a small Π_1 even for small control gains.

Case 2: $\|\zeta\| \leq \sigma$

In this case (21) yields

$$\begin{aligned} \dot{V}_3 \leq & -\{\kappa_1 \|s\|^2 + \kappa_2 \|s\|^{\rho+1}\} + \|s\| \|\varepsilon\| + \|s\| k_\zeta \zeta \\ & + s^T \Delta u \end{aligned} \quad (26)$$

that is

$$\begin{aligned} \dot{V}_3 \leq & -\{\kappa_1 \|s\|^2 + \kappa_2 \|s\|^{\rho+1}\} - \{\|\zeta\|^2 + \|\zeta\|^{\rho+1}\} \\ & + \{\|\sigma\|^2 + \|\sigma\|^{\rho+1}\} + (k_\zeta \sigma + \|\varepsilon\| + \|\Delta u\|) \|s\| \\ \leq & -\hat{\kappa}_1 V_3 - \hat{\kappa}_2 V_3^{\frac{\rho+1}{2}} + \Gamma \end{aligned} \quad (27)$$

where $\hat{\kappa}_1 = \min\{2\kappa_1, 2\}$, $\hat{\kappa}_2 = \min\{2^{\frac{\rho+1}{2}}\kappa_2, 2^{\frac{\rho+1}{2}}\}$, $\Gamma = \|\sigma\|^2 + \|\sigma\|^{\rho+1} + (k_\zeta \sigma + \|\varepsilon\| + \|\Delta u\|) \|s\|$. From Lemma 3 and the proof of Case 1, it follows that s converges to $\Pi_2 \triangleq \{(s, \zeta) \mid V_3(s, \zeta) \leq \frac{\Gamma}{2(1-\chi)\hat{\kappa}_1}\}$ in finite time.

In Theorem 1 we proved the finite-time stability of the observer. For practical systems, the estimation error \tilde{d} will not escape in finite time. According to the results presented in [31] and discussions in Step 2, the proposed sliding surface is finite-time stable.

Step 3: This step proves that the state will converge to a neighborhood of the equilibrium point along the sliding surface s . As discussed in Step 2, s converges to a neighborhood of the origin. Without loss of generality, we consider the scalar case. From previous discussions, one has $s = \dot{e} + \alpha e + \beta s_\nu(e) \leq \Pi$. Since $s_\nu(e)$ is piecewise, two scenarios are analyzed.

Case 1: $|e| \geq \delta$. In this case, one has $\dot{e} + \alpha \tilde{e} + \beta \text{sig}(e)^\nu = \hat{\Pi}$, $\hat{\Pi} \leq \Pi$, implying

$$\dot{e} + \alpha e + \left(\beta - \hat{\Pi} \text{sig}(e)^{-\nu}\right) \text{sig}(e)^\nu = 0 \quad (28)$$

$$\dot{e} + \left(\alpha - \hat{\Pi} e^{-1}\right) e + \beta \text{sig}(e)^\nu = 0. \quad (29)$$

From (28), we have $\dot{e} = -\alpha e - (\beta - \hat{\Pi} \text{sig}(e)^{-\nu}) \text{sig}(e)^\nu$. The time derivative of the Lyapunov function $V_e = \frac{1}{2} e^2$ is

$$\begin{aligned} \dot{V}_e &= -\alpha e^2 - \left(\beta - \hat{\Pi} \text{sig}(e)^{-\nu}\right) |q|^{\nu+1} \\ &= -2\alpha V_e - 2^{\frac{\nu+1}{2}} \left(\beta - \hat{\Pi} \text{sig}(e)^{-\nu}\right) V_e^{\frac{\nu+1}{2}}. \end{aligned} \quad (30)$$

Hence, if $\beta - \hat{\Pi} \text{sig}(e)^{-\nu} > 0$, i.e., $|e| > \left(\frac{\hat{\Pi}}{\beta}\right)^{1/\nu}$, then e will be finite-time stable. The convergence region and time can be calculated according to Lemma 2. Alike, one can obtain similar results from (29). In conclusion, e will converge to $\Omega \triangleq \{e \mid |e| \leq \min\left(\sqrt[\nu]{\frac{\hat{\Pi}}{\beta}}, \frac{\hat{\Pi}}{\beta}\right), |e| > \delta\}$.

Case 2: $|e| < \delta$. In this case, the tracking error is already in Ω , which can be treated as an attraction region under $|e| < \delta$. ■

IV. SIMULATION

In this section, simulations are conducted to verify the effectiveness of the proposed control scheme. We consider an extensible 3-D soft arm with its base rotated such that in a straight configuration $q = 0$ m, the robot has its tip pointing downward while being aligned with the gravitational field. In the simulations, we consider two scenarios: a) the arm being discretized with one constant curvature (CC) [23] segment and b) the arm consisting of two CC segments. We will only report the settings for the two-segment case for conciseness. The parameters for the one-segment case correspond to those of the first segment in the two-segment case.

The configuration of the soft robotic arm is defined as $q = [\Delta_{x,1} \ \Delta_{y,1} \ \delta L_1 \ \Delta_{x,2} \ \Delta_{y,2} \ \delta L_2]^T$ according to the Δ -parameterization [22] of the piecewise constant curvature (PCC) assumption. Each segment has a length of 1 m and mass of 0.3 kg. The stiffness and damping matrices are assumed diagonal and equal to $\bar{K}_i = 1$ Nm and $\bar{D}_i = 0.1$ Ns m⁻¹, $i = 1, 2$, respectively. The saturated DOSMC controller is compared with a PID+ controller [6], hereinafter GC-PID, and a traditional integral sliding mode controller [19] referred to as ISMC.

The robot starts at rest, and the simulation runs for 25 s. The lumped uncertainty, containing a time-varying term throughout the whole simulation and a perturbation term from $t = 14$ s to $t = 20$ s, is set as

$$d(t) = \begin{cases} \begin{bmatrix} s_t & c_t & s_{0.5t} & s_t & c_t & s_{0.5t} \end{bmatrix}^T, & t \in [0, 14) \cup [20, 25] \text{ s} \\ \begin{bmatrix} s_t + 4 & c_t + 4 & s_{0.5t} + 3 \\ s_t + 3 & c_t + 5 & s_{0.5t} + 3 \end{bmatrix}^T, & t \in [14, 20) \text{ s} \end{cases}$$

where $c_x = \cos x$, $s_x = \sin x$. The saturation constraints are imposed on the control inputs, i.e., $\tau \in [-\hat{\tau}, \hat{\tau}]$ with $\hat{\tau} = [10 \ 10 \ 15 \ 10 \ 10 \ 15]^T$ Nm. The commands to the controllers include three successive targets (in m)

$$q_d(t) = \begin{cases} \begin{bmatrix} 2 & 2 & 1 & -2 & -2 & 1 \end{bmatrix}^T, & 0 \leq t < 10 \text{ s} \\ \begin{bmatrix} 1 & 1 & 0.5 & -1 & -1 & 0.5 \end{bmatrix}^T, & 10 \leq t < 20 \text{ s} \\ \begin{bmatrix} 0 & 0 & 0 & 0 & 0 & 0 \end{bmatrix}^T, & t \geq 20 \text{ s}. \end{cases}$$

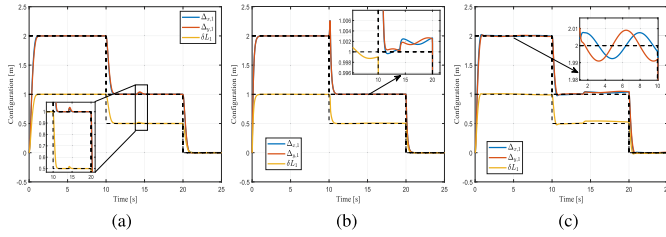


Fig. 2. Simulation results: Configuration evolution of a one segment soft robot using the three controllers. (a) Saturated DOSMC. (b) GC-PID. (c) ISMC.

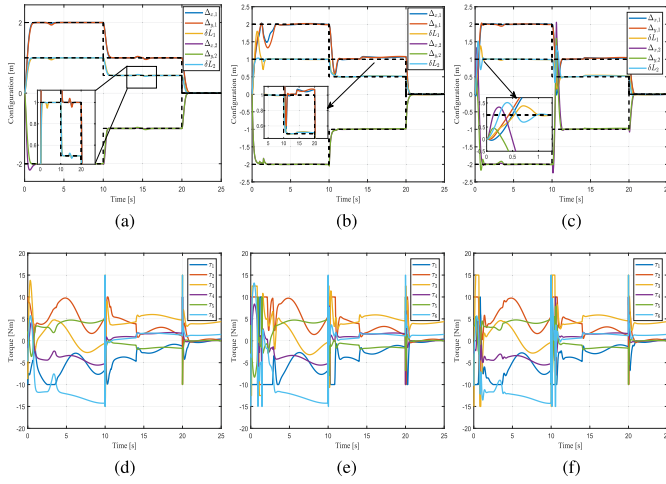


Fig. 3. Simulation results: Configuration evolution of a two-segment soft robot and inputs of the three controllers. Panels (a)–(c) plot the time evolution of the robot’s motion. Panels (d)–(f) show the control inputs. (a) and (d) Saturated DOSMC. (b) and (e) GC-PID. (c) and (f) ISMC.

When tuning the control gains, the stability of the closed-loop system has the highest priority. Given this base requirement, the tracking accuracy and response speed are considered the main performance indicators during the tuning of the control gains. The gains of the saturated DOSMC are taken as $k_1 = 9.4 \cdot I_6$, $k_2 = 5.6 \cdot I_6$, $\mu = 1.0 \cdot I_6$, $\nu = 0.55$, $\delta = 0.01$, $\alpha = \text{diag}(2.6, 2.5, 2.3, 3.1, 3.3, 2.7)$, $\beta = \text{diag}(1.9, 1.5, 1.5, 2.6, 2.8, 2.2)$, $\rho = 0.7$, $\kappa_1 = 5.4 \cdot I_6$, $\kappa_2 = \text{diag}(1.7, 1.3, 1.1, 2.3, 2.5, 2.0)$, $\hat{h}_1 = 3.0 \cdot I_6$, $\hat{h}_2 = 2.0 \cdot I_6$, $\sigma = 0.001$, and $k_\zeta = 0.7 \cdot I_6$. The gains of the GC-PID are set as $K_P = 20 \cdot I_6$, $K_D = 7.5 \cdot I_6$, and $K_I = 1.2 \cdot I_6$. For the ISMC, $k_1 = 3$, $k_2 = 1$, and $\eta = 0.01$ are chosen. The simulation results are given in Figs. 2–5.

Fig. 2 shows the configuration evolution for the one-segment case. Overall, all three controllers can track the reference commands. However, the proposed method can better deal with uncertainty, especially when the additional perturbation is applied at $t = 14 \sim 20$ s.

Figs. 3–5 illustrate the simulation results for the two-segment case. All the controllers yield stable closed-loop systems with a small tracking error. However, at the beginning of the simulation ($t = 0$ s) and the moment when the reference command is switched ($t = 8$ s), the proposed method yields better transient performance. As the additional perturbations appear at

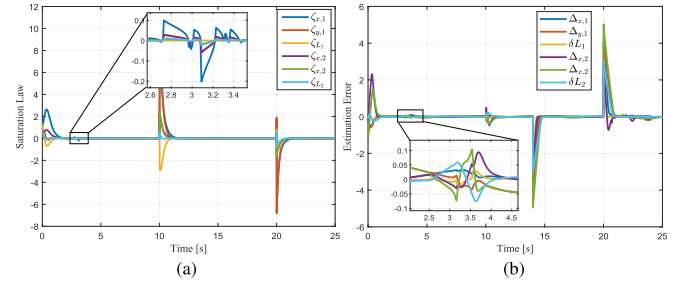


Fig. 4. Simulation results: Time evolution of the saturation law and of the observer estimation errors for the one-segment case. (a) Saturation law. (b) Estimation errors.

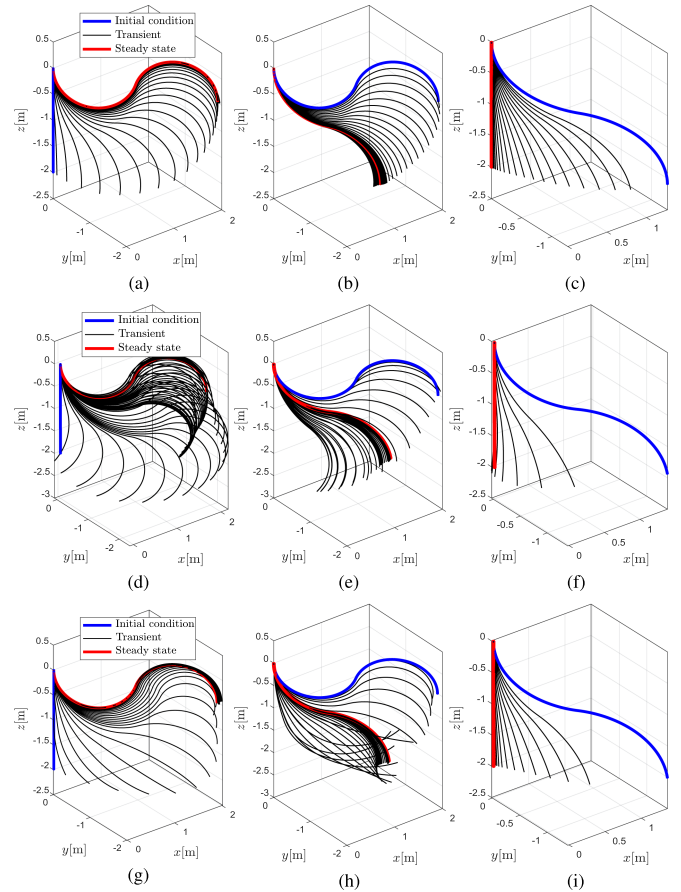


Fig. 5. Simulation results: Panels (a)–(c) plot the stroboscopic views of the motion of the two-segment soft robot under the control of the saturated DOSMC. Panels (d)–(f) show the motion while using the GC-PID regulator. Panels (g)–(i) visualize the trajectory while using the ISMC controller. (a), (d), and (g) $t \in [0, 10]$ s. (b), (e), and (h) $t \in [10, 20]$ s. (c), (f), and (i) $t \in [20, 25]$ s.

$t = 14$ s, the saturated DOSMC soon adapts to these, while the performance of the GC-PID and ISMC controllers deteriorates. Looking at the control inputs, we can observe that saturation occurs when the reference is changed. For the proposed method, the saturation law starts producing additional control signals to compensate for the saturation at these instants [see Fig. 4(a)], leading to a better transient performance. Contrarily, since both GC-PID and ISMC do not take saturation into account, the

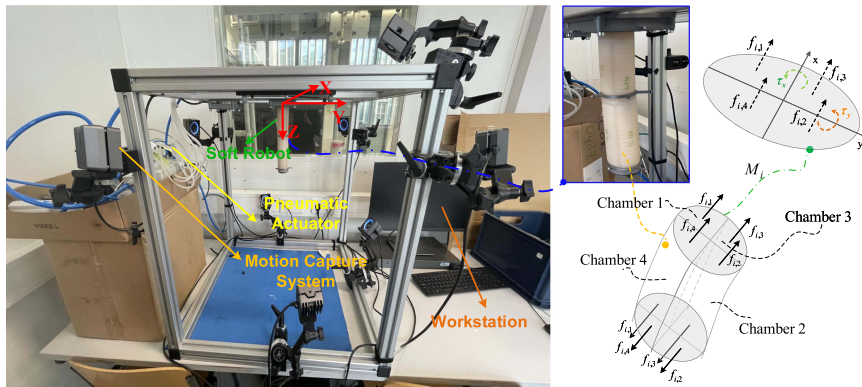


Fig. 6. Soft robotic platform used for the experiments. The left-hand side of the figure illustrates the components of the platform. The soft robot is actuated pneumatically, and the air pressure is controlled via a pressure regulator. We measure the robot's shape with a motion capture system. A workstation is used to process all the data and evaluate the controller. On the right-hand side of the picture, we zoom in on the two-segment continuum soft robot used during the experiments. We also present a schematic representation of the mapping $M_i \in \mathbb{R}^{2 \times 4}$ from the internal forces $f \in \mathbb{R}^4$ within the air cavities to the generalized wrench $\tau \in \mathbb{R}^2$ in Cartesian space used as the control input. The force f_k is applied at the center of pressure of the k th top chamber wall and proportional to both the cross-sectional area A_k and the applied pressure p_k .

performance deteriorates to varying degrees. Fig. 4(b) shows the estimation errors of the observer. The proposed observer has a fast convergence property. During $t = 14$ – 20 s, when additional perturbations are added to the system, it responds quickly, preventing the system from being significantly influenced by the disturbances. For a better illustration of the dynamic behavior in the workspace, Fig. 5 shows stroboscopic views of the motion of the soft robot for all three controllers.

V. EXPERIMENT

We present here the experimental results of the proposed DOSMC for the pneumatically actuated soft robotic platform shown in Fig. 6. A motion capture system is used to measure the SE(3) pose of the distal end of each segment, which is communicated to a workstation that runs inverse kinematics to identify the current robot configuration $q(t)$. The controller is implemented in Simulink and its control inputs are sent to a pressure regulator that actuates the robot. The soft arm is fabricated through the means of silicone casting [32] and consists of two segments, with the second segment having four active inflatable chambers. The segment length and mass are measured as 110 mm and 108 g, respectively. Under the PCC [23] assumption, we model the robot as inextensible through the Δ -parameterization [22] so that the configuration is represented by $q = [\Delta_{x,1} \ \Delta_{y,1} \ \Delta_{x,2} \ \Delta_{y,2}]^T \in \mathbb{R}^4$. The stiffness and damping matrices are identified through the same least square approach used in [24], resulting in $K = \text{diag}(1.4496, 1.4496, 1.2544, 1.2544) \text{ Nm}^{-1}$ and $D = 4.3 \times 10^{-3} \cdot \mathbf{I}_4 \text{ Nsm}^{-1}$, respectively. Since the actual inputs to the system are pressures $p_k, k = 1, \dots, 4$, the mapping from torques to pressures proposed in [33] is adopted.

Therefore, the controller output $\tau_j, j = 1, \dots, 2$; is mapped into a set of linear forces $f_i, i = 1, \dots, 4$; acting along the axial direction of each chamber at a distance d_i from the segment backbone. These are finally converted into the pressures p_k

via $f_k = p_k A_k$, where A_k is the cross-sectional area of the k th chamber. d_i and A_k are extracted from the CAD model as $d_i = 13.5$ mm and $A_k = 210$ mm², respectively.

Since the first segment is unactuated, we treat its influence on the second as a dynamic uncertainty. Note that this makes the control problem significantly more challenging compared to considering just a one-segment robot. The reference configurations for the second segment are set as (in m) as

$$q_{(3,4),d}(t) = \begin{cases} \begin{bmatrix} -0.3 & -0.3 \end{bmatrix}^T, & 0 \leq t < 8 \text{ s} \\ \begin{bmatrix} 0.2 & 0.2 \end{bmatrix}^T, & t \geq 8 \text{ s}. \end{cases} \quad (31)$$

The experiment lasts 16 s and the control loop is executed at 100 Hz. The pressure vector $p = [p_1 \ p_2 \ p_3 \ p_4]^T$ is restricted to the set $p \in [0, p_{\max}]$ with $p_{\max} = [0.55 \ 0.55 \ 0.45 \ 0.45]^T$ bar. These pressure limits can then be mapped into configuration space using the actuation matrix A_q (e.g., $\tau_{q,\max} = A_q p_{\max}$) and subsequently used in the controller.

For comparison purposes, experiments with the GC-PID and ISMC controllers are also conducted. We use the same tuning strategy to identify control gains as for the simulations. The gains of the GC-PID are chosen as $K_P = \text{diag}(0.88, 0.55)$, $K_D = \text{diag}(0.15, 0.12)$, and $K_I = \text{diag}(0.9, 0.7)$. The gains of ISMC are set to $k_1 = 3$, $k_2 = 4.5$, and $\eta = 0.01$. For the saturated DOSMC, the gains of the observer and the saturation law are the same as the simulations, while the control gains are $\nu = 0.55$, $\delta = 0.01$, $\alpha = \text{diag}(8.9, 6.7)$, $\beta = \text{diag}(4.5, 4.8)$, $\rho = 0.7$, $\kappa_1 = \text{diag}(5.1, 4.7)$, and $\kappa_2 = \text{diag}(2.3, 3.0)$. To avoid possible chattering introduced by the sgn function, the boundary layer technique proposed in [27] is adopted.

The experimental results are presented in Figs. 7–11. Figs. 7 and 8 show the evolution of system states and input pressures of GC-PID and ISMC, respectively. The closed-loop behaviors of the two controllers are comparable. Both of them can regulate the system to the preset configuration, but the transient performances are poor with long settling times (around 5 s for

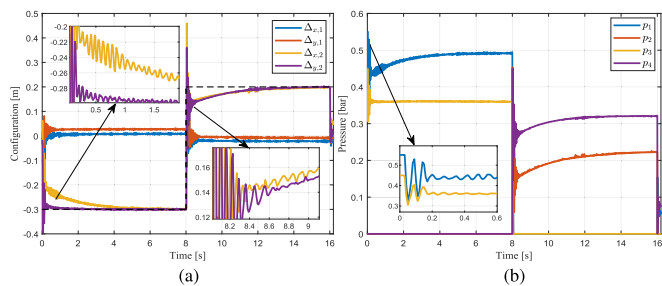


Fig. 7. Experimental results: Time evolution of the configuration variables and the input pressures for the GC-PID regulator. (a) Configuration for the GC-PID. (b) Input pressures of the GC-PID.

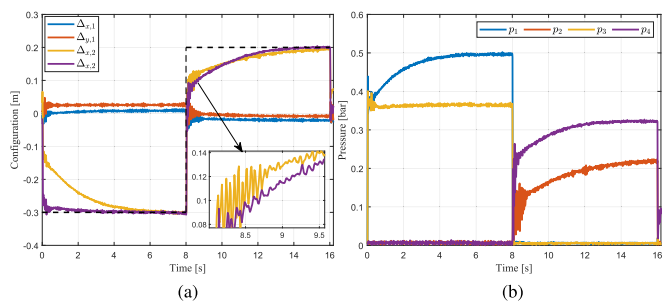


Fig. 8. Experimental results: Time evolution of the configuration variables and the input pressures for the ISMC regulator. (a) Configuration for the ISMC. (b) Input pressures of the ISMC.

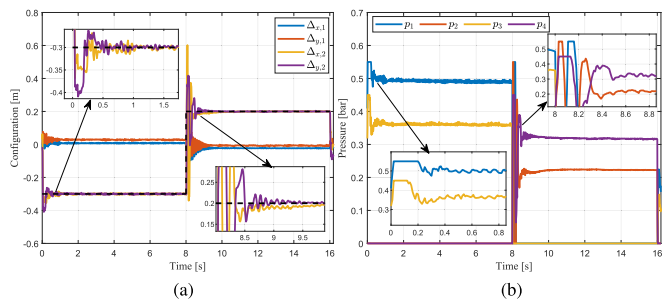


Fig. 9. Experimental results: Time evolution of the configuration variables and of the input pressures for the DOSMC without the saturation law (16). (a) Configuration for the DOSMC. (b) Input pressures for the DOSMC.

both controllers) and persistent small oscillations. Fig. 9 shows the results for the DOSMC without saturation law (16). As it is possible to observe from Fig. 9(a), the DOSMC yields significantly better performance compared to GC-PID and ISMC, the system states are smoother, and the settling time is dramatically reduced (within 0.5s). As presented in Fig. 9(b), the corresponding control inputs of the DOSMC are more aggressive than GC-PID and ISMC. This is because the observer generates additional input signals that quickly compensate for the system uncertainty, as shown in Fig. 10(c). We also tried to increase the control gains of GC-PID and ISMC to improve their transient performance, but this did not achieve better results. Note that when the reference is switched at $t = 8$ s, the DOSMC without

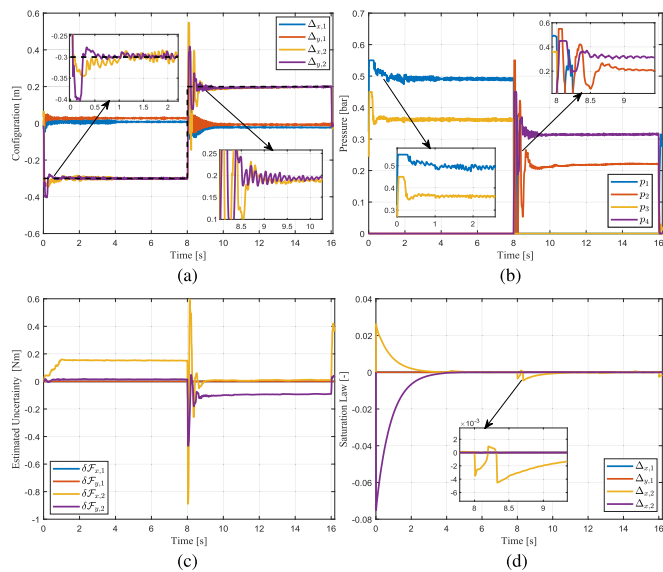


Fig. 10. Experimental results for the saturated DOSMC. Panels (a) and (c) depict the time evolution of configuration variables and input pressures. Panel (c) plots the outputs of the observer, and panel (d) shows the outputs of the saturation law. (a) States evolution. (b) Inputs pressures. (c) Observer performance. (d) Saturation law.

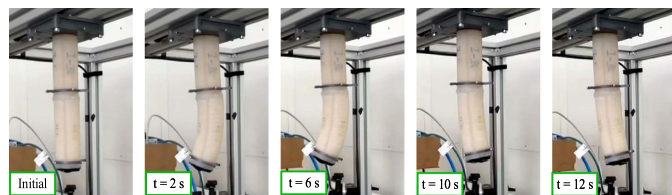


Fig. 11. Experimental results: Motion sequence of the saturated DOSMC.

saturation law is very aggressive and produces large control signals resulting in an overshooting behavior. Reducing observer and controller gains would help reduce the overshoot, but it may sacrifice performance with respect to other metrics, such as response speed and steady-state error. There exists a variety of tradeoffs for tuning the observer and controller gains, and the used gain selection strategy should always be based on the respective task requirements. While tuning the control gains in this article, we aimed for a small steady-state error and a fast response speed while accepting some overshoot. This overshoot is slightly reduced when using the saturated DOSMC instead of the plain DOSMC, as shown in Fig. 10(a). The corresponding saturation law curves are plotted in Fig. 10(d). The motion sequence of the system for the proposed controller is presented in Fig. 11 to aid the interpretation of the robot's configuration values.

VI. CONCLUSION

In this work, we proposed a model-based control architecture for shape regulation of soft robots robust to system uncertainties and can deal with input saturation. The scheme included an SMC

to steer the configuration to the desired equilibrium, an observer to estimate the system uncertainty, and an adaptive law to ensure closed-loop stability despite the presence of input saturation. We analyzed the controller from a theoretical standpoint to assess the stability in closed loop. We validated the theoretical results through simulations and experiments. Future work will extend the architecture to execute tasks involving interactions with an unstructured environment.

REFERENCES

- [1] C. Della Santina, M. G. Catalano, and A. Bicchi, "Soft robots," *Encyclopedia Robot.*, vol. 489, pp. 1–2, 2021.
- [2] C. Della Santina, C. Duriez, and D. Rus, "Model-based control of soft robots: A survey of the state of the art and open challenges," *IEEE Control Syst. Mag.*, vol. 43, no. 3, pp. 30–65, Jun. 2023.
- [3] E. Franco, "Energy shaping control of hydraulic soft continuum planar manipulators," *IEEE Contr. Syst. Lett.*, vol. 6, pp. 1748–1753, 2022.
- [4] C. M. Best, L. Rupert, and M. D. Killpack, "Comparing model-based control methods for simultaneous stiffness and position control of inflatable soft robots," *Int. J. Robot. Res.*, vol. 40, no. 1, pp. 470–493, 2021.
- [5] J. M. Bern and D. Rus, "Soft IK with stiffness control," in *Proc. IEEE 4th Int. Conf. Soft Robot.*, 2021, pp. 465–471.
- [6] P. Pustina, C. Della Santina, and A. De Luca, "Feedback regulation of elastically decoupled underactuated soft robots," *IEEE Robot. Automat. Lett.*, vol. 7, no. 2, pp. 4512–4519, Apr. 2022.
- [7] X. Zheng, H. Huang, J. Wang, X. Zhao, and Q. Xu, "Behavioral decision-making model of the intelligent vehicle based on driving risk assessment," *Comput.-Aided Civil Infrastructure Eng.*, vol. 36, no. 7, pp. 820–837, 2021.
- [8] C. Armanini, F. Boyer, A. T. Mathew, C. Duriez, and F. Renda, "Soft robots modeling: A structured overview," *IEEE Trans. Robot.*, vol. 39, no. 3, pp. 1728–1748, Jun. 2023.
- [9] S. Sadati, S. E. Naghibi, L. Da Cruz, and C. Bergeles, "Reduced-order modeling and model order reduction for soft robots," 2021.
- [10] J. Till, V. Aloï, and C. Rucker, "Real-time dynamics of soft and continuum robots based on Cosserat rod models," *Int. J. Robot. Res.*, vol. 38, no. 6, pp. 723–746, 2019.
- [11] V. Cacucciolo, J. Shintake, Y. Kuwajima, S. Maeda, D. Floreano, and H. Shea, "Stretchable pumps for soft machines," *Nature*, vol. 572, no. 7770, pp. 516–519, 2019.
- [12] X. Shao, G. Sun, W. Yao, J. Liu, and L. Wu, "Adaptive sliding mode control for quadrotor UAVs with input saturation," *IEEE/ASME Trans. Mechatron.*, vol. 27, no. 3, pp. 1498–1509, Jun. 2022.
- [13] H. Dong, X. Yang, and M. V. Basin, "Practical tracking of permanent magnet linear motor via logarithmic sliding mode control," *IEEE/ASME Trans. Mechatron.*, vol. 27, no. 5, pp. 4112–4121, Oct. 2022.
- [14] S. K. Spurgeon, "Sliding mode observers: A survey," *Int. J. Syst. Sci.*, vol. 39, no. 8, pp. 751–764, 2008.
- [15] S. Chaudhari, P. D. Shendge, and S. B. Phadke, "Disturbance observer based controller under noisy measurement for tracking of nDOF uncertain mismatched nonlinear interconnected systems," *IEEE/ASME Trans. Mechatron.*, vol. 25, no. 3, pp. 1600–1611, Jun. 2020.
- [16] J. T. Moura, H. Elmali, and N. Olgac, "Sliding mode control with sliding perturbation observer," *J. Dyn. Syst., Meas., Control*, vol. 119, no. 4, pp. 657–665, Dec. 1997.
- [17] H. Khan, S. J. Abbasi, K. D. Kallu, H. H. Kim, Y.-J. An, and M. C. Lee, "Robust position control of assistive robot for paraplegics," *Int. J. Control, Automat. Syst.*, vol. 19, no. 11, pp. 3741–3752, 2021.
- [18] A. Kazemipour, O. Fischer, Y. Toshimitsu, K. W. Wong, and R. K. Katzschmann, "Adaptive dynamic sliding mode control of soft continuum manipulators," in *Proc. Int. Conf. Robot. Automat. (ICRA)*, 2022, pp. 3259–3265.
- [19] A. H. Khan and S. Li, "Sliding mode control with PID sliding surface for active vibration damping of pneumatically actuated soft robots," *IEEE Access*, vol. 8, pp. 88793–88800, 2020.
- [20] G. Cao, Y. Liu, Y. Jiang, F. Zhang, G. Bian, and D. H. Owens, "Observer-based continuous adaptive sliding mode control for soft actuators," *Nonlinear Dyn.*, vol. 105, no. 1, pp. 371–386, 2021.
- [21] J.-J. Slotine and S. S. Sastry, "Tracking control of non-linear systems using sliding surfaces, with application to robot manipulators," *Int. J. Control*, vol. 38, no. 2, pp. 465–492, 1983.
- [22] C. Della Santina, A. Bicchi, and D. Rus, "On an improved state parametrization for soft robots with piecewise constant curvature and its use in model based control," *IEEE Robot. Automat. Lett.*, vol. 5, no. 2, pp. 1001–1008, Apr. 2020.
- [23] R. J. Webster III and B. A. Jones, "Design and kinematic modeling of constant curvature continuum robots: A review," *Int. J. Robot. Res.*, vol. 29, no. 13, pp. 1661–1683, 2010.
- [24] C. Della Santina, R. K. Katzschmann, A. Bicchi, and D. Rus, "Model-based dynamic feedback control of a planar soft robot: Trajectory tracking and interaction with the environment," *Int. J. Robot. Res.*, vol. 39, no. 4, pp. 490–513, 2020.
- [25] G. Zheng, "Control of a silicone soft tripod robot via uncertainty compensation," *IEEE Robot. Automat. Lett.*, vol. 5, no. 2, pp. 2801–2807, Apr. 2020.
- [26] J. Chang, J. Cieslak, Z. Guo, and D. Henry, "On the synthesis of a sliding-mode-observer-based adaptive fault-tolerant flight control scheme," *ISA Trans.*, vol. 111, pp. 8–23, 2021.
- [27] S. Yu, X. Yu, B. Shirinzadeh, and Z. Man, "Continuous finite-time control for robotic manipulators with terminal sliding mode," *Automatica*, vol. 41, no. 11, pp. 1957–1964, 2005.
- [28] J. Yu, P. Shi, and L. Zhao, "Finite-time command filtered backstepping control for a class of nonlinear systems," *Automatica*, vol. 92, pp. 173–180, 2018.
- [29] E. Cruz-Zavala, J. A. Moreno, and L. M. Fridman, "Uniform robust exact differentiator," *IEEE Trans. Autom. Control*, vol. 56, no. 11, pp. 2727–2733, Nov. 2011.
- [30] K. Lu and Y. Xia, "Adaptive attitude tracking control for rigid spacecraft with finite-time convergence," *Automatica*, vol. 49, no. 12, pp. 3591–3599, 2013.
- [31] J. Yang, S. Li, J. Su, and X. Yu, "Continuous nonsingular terminal sliding mode control for systems with mismatched disturbances," *Automatica*, vol. 49, no. 7, pp. 2287–2291, 2013.
- [32] A. D. Marchese, R. K. Katzschmann, and D. Rus, "A recipe for soft fluidic elastomer robots," *Soft Robot.*, vol. 2, no. 1, pp. 7–25, 2015.
- [33] C. Della Santina, A. Bicchi, and D. Rus, "Dynamic control of soft robots with internal constraints in the presence of obstacles," in *Proc. IEEE/RSJ Int. Conf. Intell. Robots Syst.*, 2019, pp. 6622–6629.



Xiangyu Shao received the B.S. degree in automation from Harbin Engineering University, Harbin, China, in 2016, and M.S. and Ph.D. degrees in control science and engineering from the Harbin Institute of Technology, Harbin, China, in 2018 and 2022, respectively.

He is currently an Assistant Professor with the School of Astronautics, Harbin Institute of Technology. His research interests include space robots, soft robots, sliding mode control, and fractional order control.



Pietro Pustina (Graduate Student Member) received the B.S. degree in computer engineering from the University of Roma Tre, Rome, Italy, in 2019, and the M.S. degree in control engineering from the Sapienza University of Rome, Rome, Italy, in 2021, where he has been working toward the Ph.D. degree in automatic control since 2021.

His research interests include modeling and control of continuum soft robots.



Maximilian Stölzle received the B.S. degree in mechanical engineering and the M.S. degree with distinction in mechanical engineering from the Swiss Federal Institute of Technology Zurich, Zurich, Switzerland, in 2019 and 2021, respectively. He is currently working toward the Ph.D. degree in robotics with the Department of Cognitive Robotics, Faculty of Mechanical, Maritime, and Materials Engineering, Delft University of Technology, Delft, The Netherlands.

His research interest includes the modeling, sensing, and control of soft robots.



Guanghui Sun (Senior Member, IEEE) received the B.S. degree in automation and the M.S. and Ph.D. degrees in control science and engineering from the Harbin Institute of Technology, Harbin, China, in 2005, 2007, and 2010, respectively.

He is currently a Professor with the Department of Control Science and Engineering, Harbin Institute of Technology. His research interests include fractional-order systems, networked control systems, and sliding mode control.



Alessandro De Luca (Life Fellow, IEEE) received the Ph.D. degree in systems engineering from Sapienza University of Rome, Rome, Italy, in 1987. He is a Professor of robotics and automation with the Sapienza University of Rome, Rome, Italy. His research interests include modeling, motion planning, and control of robotic systems (flexible manipulators, kinematically redundant arms, underactuated robots, wheeled mobile robots), as well as physical human–robot interaction.

Mr. Luca was the recipient of the three conference awards (Best paper at ICRA 1998 and BioRob 2012, Best application paper at IROS 2008), the Helmholtz Humboldt Research Award in 2005, the IEEE-RAS Distinguished Service Award in 2009, and the IEEE George Saridis Leadership Award in Robotics and Automation in 2019. He was the Scientific Coordinator of the FP7 project SAPHARI—Safe and Autonomous Physical Human–Aware Robot Interaction (2011–15). He has been the first Editor-in-Chief of the IEEE TRANSACTIONS ON ROBOTICS (2004–08), RAS Vice-President for Publication Activities in 2012–13, General Chair of ICRA 2007, and Program Chair of ICRA 2016.



Ligang Wu (Fellow, IEEE) received the B.S. degree in automation from the Harbin University of Science and Technology, Harbin, China, in 2001, the M.E. degree in navigation guidance and control, and the Ph.D. degree in control theory and control engineering from the Harbin Institute of Technology, China in 2003 and 2006, respectively.

From 2006 to 2007, he was a Research Associate with the Department of Mechanical Engineering, The University of Hong Kong, Hong Kong. From 2007 to 2008, he was a Senior Research Associate with the Department of Mathematics, City University of Hong Kong, Hong Kong. From 2012 to 2013, he was a Research Associate with the Department of Electrical and Electronic Engineering, Imperial College London, London, U.K. In 2008, he was with the Harbin Institute of Technology, China, as an Associate Professor, and was then promoted to a Full Professor in 2012. He has authored or coauthored seven research monographs and more than 170 research papers in internationally referred journals. His research interests include switched systems, stochastic systems, computational and intelligent systems, sliding mode control, and advanced control techniques for power electronic systems.

Dr. Wu was the winner of the National Science Fund for Distinguished Young Scholars in 2015 and recipient of the China Young Five Four Medal in 2016. He was the Distinguished Professor of Chang Jiang Scholar in 2017 and was he Highly Cited Researcher in 2015–2019. He is currently an Associate Editor for several journals, including IEEE TRANSACTIONS ON AUTOMATIC CONTROL, IEEE/ASME TRANSACTIONS ON MECHATRONICS, IEEE TRANSACTIONS ON INDUSTRIAL ELECTRONICS, *Information Sciences*, *Signal Processing*, and *IET Control Theory and Applications*. He is an Associate Editor for the Conference Editorial Board, IEEE Control Systems Society.



Cosimo Della Santina (Senior Member, IEEE) received the Ph.D. degree in robotics from the University of Pisa, Pisa, Italy, in 2019.

He is currently an Assistant Professor with the Department of Cognitive Robotics, Delft University of Technology, Delft, The Netherlands. From 2017 to 2019, he was a Visiting Ph.D. Student and a Postdoctoral Researcher with the Massachusetts Institute of Technology, Cambridge, MA, USA. He was a Senior Postdoc with the Department of Informatics, Technical University of Munich, Munich, Germany, in 2020, where he became a Guest Lecturer, until 2021. Since 2020, he has been affiliated with the German Aerospace Centre (DLR) as an External Research Scientist. His research interest is in motor intelligence of physical systems, focusing on mechanical systems, high dimensional dynamics, and soft robots.